Dynamics of self-interstitial atoms in bcc metals

P. N. Ram
Department of Physics, North-Eastern Hill University, Shillong 793 003, Meghalaya, India
(Received 19 October 1990)

We present calculations of the local frequency spectrum of ⟨110⟩-split-interstitial atoms in bcc metals with the use of the Green's-function method. The dumbbell vibrates with low-frequency resonant modes and high-frequency localized modes with little contribution from the host frequencies. In agreement with experiment the spectrum leads to enhanced mean-square thermal displacements of the dumbbell atom. The frequencies of the librational modes B_{1g} and B_{2g} provide a consistent explanation of the observed changes in the shear moduli of irradiated Mo. The long-range migration of the interstitial atoms is discussed in view of the obtained resonance modes.

I. INTRODUCTION

The dynamical behavior of self-interstitial atoms (SIA's) is of considerable interest in understanding the properties of irradiated metals. The properties of SIA's in fcc metals including their stable configuration and dynamics are fairly well understood.[1–4] Especially interesting is the occurrence of resonance modes[5] of SIA's which are instrumental in explaining the physical properties of irradiated metals.[1–8] They provide simple physical interpretation to interstitial elementary jumping processes with low activation energy and lead to high shear polarizability of SIA's. The earlier expectation[7] of the direct observation of the resonance modes in diffuse inelastic neutron scattering has now been realized with the measurements on electron-irradiated Al.[9]

In the case of bcc metals the symmetry and structure of SIA's have been studied by computer simulation and the ⟨110⟩-dumbbell configuration, at least in α-Fe,[10–12] Mo,[12,13] and W,[12,14] has been found. Experimentally, the ⟨110⟩-dumbbell configuration has been confirmed by x-ray diffuse scattering in Mo (Ref. 15) and α-Fe,[16,17] by internal friction measurements in Mo,[18] W,[19] and α-Fe,[20] by elastic aftereffect in α-Fe (Ref. 21) and W,[22] and by magnetic aftereffect in α-Fe.[23] But the studies on the dynamical behavior of this defect have not been reported. Similar to the ⟨100⟩ dumbbell in fcc metals the ⟨110⟩ dumbbell in bcc metals is expected to vibrate with characteristic low-frequency resonance modes[3,24] and high-frequency localized modes. Recent Mössbauer study on trapped interstitials in Mo gives clear hints for the existence of low-frequency resonance modes of the ⟨110⟩ dumbbell.[25]

In this paper we report the calculation of dynamics of the ⟨110⟩-dumbbell interstitials in a bcc metal presenting the local frequency spectrum of the defect in Mo which shows the occurrence of both kinds of characteristic modes. The case of Mo is of special interest, since there seems to be some controversy about the interpretation of resistivity recovery and long-range migration of SIA's.[24,26–29] While computer simulation[1,12] favors a three-dimensional migration involving reorientation of the dumbbell axis no such reorientation is observed in elastic aftereffect measurements.[26] The long-range migration of SIA's is supposed to be mediated by the libration mode of a dumbbell having strong displacements in the $(1\bar{1}0)$ plane[26] while observed strong reduction in shear modulus C' of irradiated Mo indicates strongest softening of the lattice in the $[1\bar{1}0]$ direction.[27] The dynamics of the ⟨110⟩ dumbbell would be of immense help in clarifying the situation and is expected to give much needed insight in understanding the behavior of SIA's in bcc metals.

II. LOCAL DENSITY OF STATES

In a defect-lattice dynamical study the basic quantity of interest is the lattice Green's function for the defect crystal. One of the most important consequences of the presence of defects in solids is the excitation of the characteristic modes of the defect, i.e., localized and resonance modes. The occurrence of a resonance mode is signaled by an increase in the density of states near the resonant frequency, which is generally observed as resonant-type peaks in the frequency spectrum of the defect crystal, whereas the localized modes are identified as additional peaks in the spectrum. The density of states can be expressed in terms of the Green's function of the lattice. Very often the characteristic modes are dominated by the vibrations of the defect and a few of its neighbors. In such a situation the local representation of the density of states is more suitable where the total frequency spectrum of the lattice is expressed as the sum of the local spectra of all the atoms in the lattice. Especially interesting is the Green's function at the defect site whose imaginary part represents the local density of states of the defect. Thus the resonant vibrations of the defect are best described by the defect Green's function $G_{\alpha\alpha}(d,d;\omega)$ which is the dynamic response of the defect d, i.e., its displacement in the αth direction due to a unit force with frequency ω acting on the defect d in the direction α. The local density of states of the defect d for vibrations in the α direction is given by[7]

$$Z_\alpha(d,\omega)=\frac{2\omega M_d}{\pi}\mathrm{Im}G_{\alpha\alpha}(d,d;\omega)\ , \tag{1}$$

where M_d is the mass of the defect atom. If we write the imaginary part of the same site Green's function in terms of the eigenvectors and eigenfrequencies of the lattice it is easily seen that $Z_\alpha(d,\omega)$ gives the number of frequencies in the interval $(\omega,\omega,+d\omega)$ multiplied by the square of the amplitude of atom d in the α direction. Thus the local density of states is the quantitative measure of the number of modes contributing to the vibrational behavior of the atom d. In a defect lattice $Z_\alpha(d,\omega)$ will, in general, be different for each direction and therefore the local density of states of the defect is defined by the average

$$Z(d,\omega)=\frac{2\omega M_d}{3\pi}\sum_\alpha \mathrm{Im}G_{\alpha\alpha}(d,d;\omega)\ . \tag{2}$$

The concept of local density of states is quite useful in the context of the defect-lattice dynamics. In fact, the local frequency spectrum of a defect completely describes the vibrational behavior of the defect atom. It is particularly useful for calculating those vibrational properties of the defective crystal which do not depend on correlations of different atoms, e.g., mean-square thermal displacement, defect contribution to thermodynamic quantities like entropy and lattice specific heat, etc.

We discuss the local frequency spectrum of the $\langle 110\rangle$ dumbbell using the standard Green's-function method for the interstitials.[2] The entire space is divided into two subspaces: a central subspace $\mathbb{C}$ consisting of the dumbbell atoms and a subspace $\mathbb{R}$ containing the rest of the lattice atoms. The defect Green's function $G_{\alpha\alpha}(d,d;\omega)$ can be obtained from that for the interstitial subspace

$$G_{CC}(\omega)=[\Phi_{CC}-\Phi_{CR}\hat{G}_{RR}(\omega)\Phi_{RC}-M_{CC}\omega^2]^{-1}\ , \tag{3}$$

where Φ_{CC} is the Einstein force-constant matrix for the subspace $\mathbb{C}$, Φ_{CR} is the force-constant matrix coupling the subspace $\mathbb{C}$ to host space R. It is observed that Eq. (3) has the form of the Einstein approximation for the interstitial region where the correction $-\Phi_{CR}\hat{G}_{RR}(\omega)\Phi_{RC}$ to the Einstein term Φ_{CC} describes the effect of the dynamic relaxations of the atoms in the rest lattice. For the case of the interstitial the subspace $\mathbb{R}$ contains all the atoms of the ideal lattice and $\hat{G}_{RR}=(\Phi_{RR}-M_{RR}\omega^2)^{-1}$ can easily be calculated in terms of the ideal lattice Green's function and the force-constant change matrix V_{RR} for the subspace $\mathbb{R}$ when the interstitial is kept fixed. The function $\hat{G}_{RR}$ is calculated in exactly the same way one calculates the defect-lattice Green's function for the case of substitutional impurities

$$\hat{G}_{RR}=G^0-G^0\hat{t}G^0\ , \tag{4}$$

where the t matrix is given by

$$\hat{t}=V_{RR}(1+G^0V_{RR})^{-1}\ , \tag{5}$$

with

$$V_{RR}=\Phi_{RR}-\Phi^0-(M_{RR}-M)\omega^2\ .$$

In Eqs. (4) and (5) quantities with superscript zero refer to the ideal lattice. In the present case the defect mass M_d is just equal to the host atom mass M.

We use a defect model with second-nearest-neighbor interactions. In a recent study the problem of self-interstitials in cubic metals has been discussed in detail where complete group-theoretic analysis of second-neighbor defect models for the $\langle 100\rangle$ dumbbell in the fcc lattice and the $\langle 110\rangle$ dumbbell in the bcc lattice has been presented.[30] The $\langle 110\rangle$-dumbbell configuration in the bcc lattice is shown in Fig. 1. The defect is described by an assumed vacancy at the origin and interstitial atoms at $(\pm x,\pm x,0)a/2$ where a is the lattice constant. In this model the dumbbell is surrounded by 8 nearest neighbors and 6 second-nearest-neighbors and as such the defect space consists of 17 sites and one has to deal with 51×51 matrices. In order to reduce the complexity of the calculation the orthorhombic symmetry (point group D_{2h}) of the $\langle 110\rangle$ dumbbell is used to obtain symmetry coordinates for the interstitial and its neighbors. The required symmetry coordinates are given in Table I. The defect space is decomposed as

$$\Gamma_{\mathrm{tot}}=8A_g+5B_{1g}+6B_{2g}+5B_{3g}+3A_u+8B_{1u}+8B_{2u}+8B_{3u}\ . \tag{6}$$

The dumbbell motion occurs in all the modes except B_{3g} and A_u. The defect Green's function can be projected in different subspaces of the defect space:

$$G_{\alpha\alpha}(d,d;\omega)=\langle d\alpha|G(\omega)|d\alpha\rangle=\sum_\Gamma\sum_{\mu=1}^{d_\Gamma}\sum_{j,j'=1}^{\sigma_\Gamma}\langle d\alpha|\Gamma\mu j\rangle\langle\Gamma\mu j|G(\omega)|\Gamma\mu j'\rangle\langle\Gamma\mu j'|d\alpha\rangle\ , \tag{7}$$

where σ_Γ gives the number of times that the Γth irreducible representation with the dimension d_Γ occurs in the total representation Γ_{2h}. With the help of the symmetry coordinates $U(\Gamma\mu j)=|\Gamma\mu j)$ the coefficients $\langle d\alpha|\Gamma\mu j\rangle$ are readily evaluated, facilitating the calculation of the defect Green's function in terms of the Green's functions G^Γ_{CC} of the interstitial subspace for different irreducible representations. The C-space Green's function G^Γ_{CC} for each irreducible representation Γ reduces to a scalar. In terms of G^Γ_{CC} the elements of the defect Green's function are

$$\begin{aligned}G_{xx}(d,d;\omega)&=G_{yy}(d,d;\omega)\\&=\tfrac{1}{4}(G^{A_g}_{CC}+G^{B_{1g}}_{CC}+G^{B_{2u}}_{CC}+G^{B_{3u}}_{CC})\ ,\\G_{zz}(d,d;\omega)&=\tfrac{1}{2}(G^{B_{2g}}_{CC}+G^{B_{1u}}_{CC})\ .\end{aligned} \tag{8}$$

The local density of states of the defect is given by

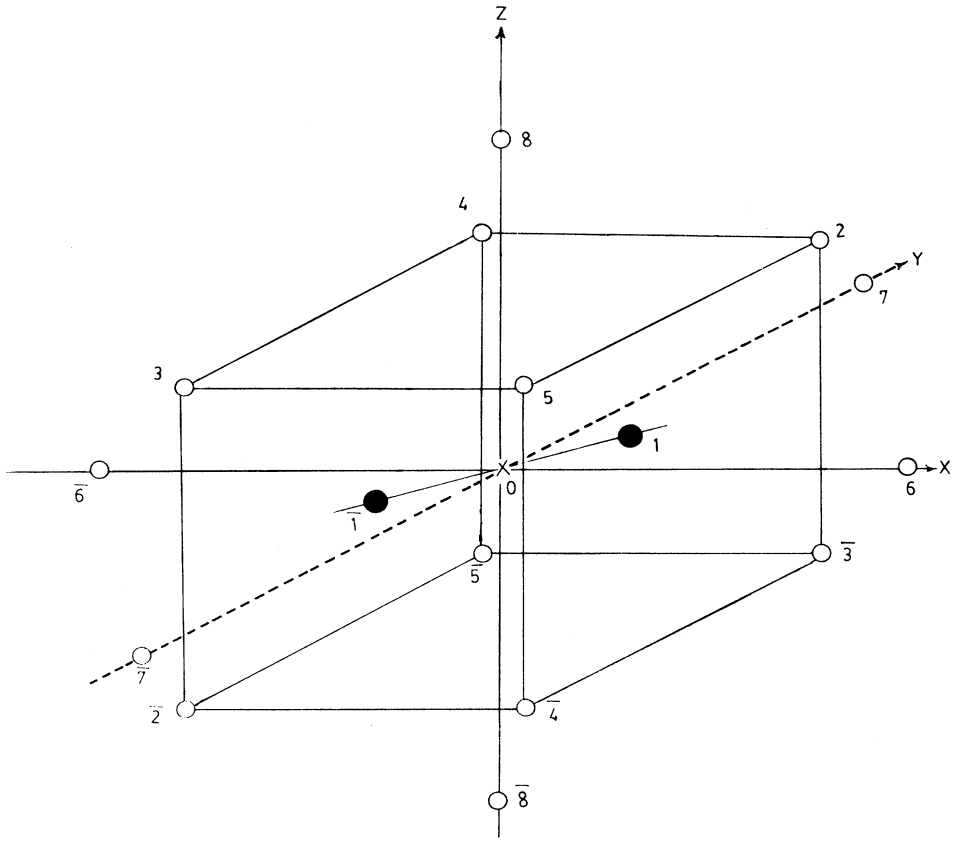

FIG. 1. ⟨110⟩-dumbbell configuration in the bcc lattice.

$$Z(d,\omega)=\tfrac{1}{3}\sum_{\alpha} Z_{\alpha}(d,\omega)$$
$$=\frac{\omega M}{3\pi}\mathrm{Im}(G_{CC}^{A_g}+G_{CC}^{B_{1g}}+G_{CC}^{B_{2g}}+G_{CC}^{B_{1u}}+G_{CC}^{B_{2u}}+G_{CC}^{B_{3u}}) . \quad (9)$$

We consider a longitudinal force constant A and a transverse force constant B for interaction between two atoms. In the highly compressed region near the interstitial the force constants are very large, and even the transverse force constants become comparable to nearest-neighbor longitudinal force constant A_1^0 in the ideal lattice. However, due to repulsion of the atoms the transverse force constants are always negative. In fact, the typical low-frequency resonance modes of SIA's are results of only these negative transverse force constants.[5] As far as the vibrations of the ⟨110⟩ dumbbell are concerned, from the elements of the defect Green's function $G(d,d;\omega)$ and the symmetry coordinates we see that the dumbbell atoms move parallel to its axis in A_g and B_{3u} modes and perpendicular to it in all the other modes. In B_{1g} and B_{2u} modes dumbbell atoms move along $[1\bar{1}0]$ while in B_{2g} and B_{1u} modes they move along the Z direction. The motion of dumbbell atoms and its four nearest neighbors in the $(1\bar{1}0)$ plane in different modes has been depicted in Fig. 2. As is evident from Fig. 2, the force constants between the dumbbell atoms are involved only in the case of even modes (A_g, B_{1g}, and B_{2g}). While in the case of the A_g mode the dominant longitudinal force constant between dumbbell atoms is involved and the relatively weak transverse force constant is not important, in

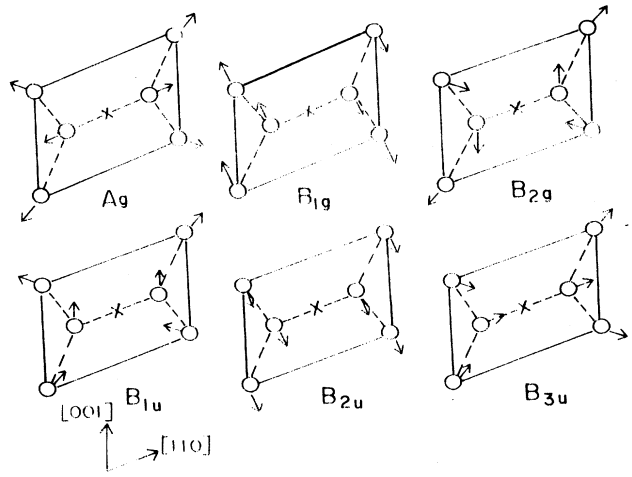

FIG. 2. Vibrational modes of the ⟨110⟩ dumbbell in the bcc lattice: localized (A_g) and resonance modes.

TABLE I. Symmetry coordinates in defect space of the ⟨110⟩ dumbbell in the bcc lattice. $U(l\alpha)$ is the amplitude of displacement of the lth atom in the αth direction. See Fig. 1 for identifying different atoms.

Representation	Symmetry coordinates
A_g	$U(A_g,1)=\frac{1}{2}[U(1x)+U(1y)-U(\bar{1}x)-U(\bar{1}y)]$
	$U(A_g,2)=(1/8^{1/2})[U(2x)+U(2y)-U(3x)-U(3y)-U(\bar{2}x)-U(\bar{2}y)+U(\bar{3}x)+U(\bar{3}y)]$
	$U(A_g,3)=\frac{1}{2}[U(2z)+U(3z)-U(\bar{2}z)-U(\bar{3}z)]$
	$U(A_g,4)=(1/8^{1/2})[-U(4x)+U(4y)+U(5x)-U(5y)+U(\bar{4}x)-U(\bar{4}y)-U(\bar{5}x)+U(\bar{5}y)]$
	$U(A_g,5)=\frac{1}{2}[U(4z)+U(5z)-U(\bar{4}z)-U(\bar{5}z)]$
	$U(A_g,6)=\frac{1}{2}[U(6x)+U(7y)-U(\bar{6}x)-U(\bar{7}y)]$
	$U(A_g,7)=\frac{1}{2}[U(6y)+U(7x)-U(\bar{6}y)-U(\bar{7}x)]$
	$U(A_g,8)=(1/2^{1/2})[U(8z)-U(\bar{8}z)]$
B_{1g}	$U(B_{1g},1)=\frac{1}{2}[U(1x)-U(1y)-U(\bar{1}x)+U(\bar{1}y)]$
	$U(B_{1g},2)=(1/8^{1/2})[U(2x)-U(2y)-U(3x)+U(3y)-U(\bar{2}x)+U(\bar{2}y)+U(\bar{3}x)-U(\bar{3}y)]$
	$U(B_{1g},3)=(1/8^{1/2})[-U(4x)-U(4y)+U(5x)+U(5y)+U(\bar{4}x)+U(\bar{4}y)-U(\bar{5}x)-U(\bar{5}y)]$
	$U(B_{1g},4)=\frac{1}{2}[U(6x)-U(7y)-U(\bar{6}x)+U(\bar{6}x)+U(\bar{7}y)]$
	$U(B_{1g},5)=\frac{1}{2}[U(6y)-U(7x)-U(\bar{6}y)+U(\bar{7}x)]$
B_{2g}	$U(B_{2g},1)=(1/2^{1/2})[U(1z)-U(\bar{1}z)]$
	$U(B_{2g},2)=(1/8^{1/2})[U(2x)+U(2y)+U(3x)+U(3y)-U(\bar{2}x)-U(\bar{2}y)-U(\bar{3}x)-U(\bar{3}y)]$
	$U(B_{2g},3)=\frac{1}{2}[U(2z)-U(3z)-U(\bar{2}z)+U\bar{3}z)]$
	$U(B_{2g},4)=(1/8^{1/2})[U(4x)+U(4y)+U(5x)+U(5y)-U(\bar{4}x)-U(\bar{4}y)-U(\bar{5}x)-U(\bar{5}y)]$
	$U(B_{2g},5)=\frac{1}{2}[U(6z)+U(7z)-U(\bar{6}z)-U(\bar{7}z)]$
	$U(B_{2g},6)=\frac{1}{2}[U(8x)+U(8y)-U(\bar{8}x)-U(\bar{8}y)]$
B_{3g}	$U(B_{3g},1)=(1/8^{1/2})[u(2x)-U(2y)+U(3x)-U(3y)-U(\bar{2}x)+U(\bar{2}y)-U(\bar{3}x)+U(\bar{3}y)]$
	$U(B_{3g},2)=(1/8^{1/2})[U(4x)-U(4y)+U(5x)-U(5y)-U(\bar{4}x)+U(\bar{4}y)-U(\bar{5}x)+U(\bar{5}y)]$
	$U(B_{3g},3)=\frac{1}{2}[-U(4z)+U(5z)+U(\bar{4}z)-U(\bar{5}z)]$
	$U(B_{3g},4)=\frac{1}{2}[U(6z)-U(7z)-U(\bar{6}z)+U(\bar{7}z)]$
	$U(B_{3g},5)=\frac{1}{2}[U(8x)-U(8y)-U(\bar{8}x)+U(\bar{8}y)]$
A_u	$U(A_u,1)=(1/8^{1/2})[U(2x)-U(2y)-U(3x)+U(3y)+U(\bar{2}x)-U(\bar{2}y)-U(\bar{3}x)+U(\bar{3}y)]$
	$U(A_u,2)=(1/8^{1/2})[-U(4x)-U(4y)+U(5x)+U(5y)-U(\bar{4}x)-U(\bar{4}y)+U(\bar{5}x)+U(\bar{5}y)]$
	$U(A_u,3)=\frac{1}{2}[U(6z)-U(7z)+U(\bar{6}z)-U(\bar{7}z)]$
B_{1u}	$U(B_{1u},1)=(1/2^{1/2})[U(1z)+U(\bar{1}z)]$
	$U(B_{1u},2)=U(0z)$
	$U(B_{1u},3)=(1/8^{1/2})[U(2x)+U(2y)-U(3x)-U(3y)+U(\bar{2}x)+U(\bar{2}y)-U(\bar{3}x)-U(\bar{3}y)]$
	$U(B_{1u},4)=\frac{1}{2}[U(2z)+U(3z)+U(\bar{2}z)+U(\bar{3}z)]$
	$U(B_{1u},5)=(1/8^{1/2})[-U(4z)+U(4y)+U(5x)-U(5y)-U(\bar{4}x)+U(\bar{4}y)+U(\bar{5}x)-U(\bar{5}y)]$
	$U(B_{1u},6)=\frac{1}{2}[U(4z)+U(5z)+U(\bar{4}z)+U(\bar{5}z)]$
	$U(B_{1u},7)=\frac{1}{2}[U(6z)+U(7z)+U(\bar{6}z)+U(\bar{7}z)]$
	$U(B_{1u},8)=(1/2^{1/2})[U(8z)+U(\bar{8}z)]$
B_{2u}	$U(B_{2u},1)=\frac{1}{2}[U(1x)-U(1y)+U(\bar{1}x)-U(\bar{1}y)]$
	$U(B_{2u},2)=(1/2^{1/2})[U(0x)-U(0y)]$
	$U(B_{2u},3)=(1/8^{1/2})[U(2x)-U(2y)+U(3x)-U(3y)+U(\bar{2}x)-U(\bar{2}y)+U(\bar{3}x)-U(\bar{3})]$
	$U(B_{2u},4)=(1/8^{1/2})[U(4x)-U(4y)+U(5x)-U(5y)+U(\bar{4}x)-U(\bar{4}y)+U(\bar{5}x)-U(\bar{5}y)]$
	$U(B_{2u},5)=\frac{1}{2}[-U(4z)+U(5z)-U(\bar{4}z)+U(\bar{5}z)]$
	$U(B_{2u},6)=\frac{1}{2}[U(6x)-U(7y)+U(\bar{6}x)-U(\bar{7}y)]$
	$U(B_{2u},7)=\frac{1}{2}[U(6y)-U(7x)+U(\bar{6}y)-U(\bar{7}x)]$
	$U(B_{2u},8)=\frac{1}{2}[U(8x)-U(8y)+U(\bar{8}x)-U(\bar{8}y)]$

TABLE I. (*Continued*).

Representation	Symmetry coordinates
B_{3u}	$U(B_{3u},1)=\frac{1}{2}[U(1x)+U(1y)+U(\bar{1}x)+U(\bar{1}y)]$
	$U(B_{3u},2)=(1/2^{1/2})[U(0x)+U(0y)]$
	$U(B_{3u},3)=(1/8^{1/2})[U(2x)+U(2y)+U(3x)+U(3y)+U(\bar{2}x)+U(\bar{2}y)+U(\bar{3}x)+U(\bar{3}y)]$
	$U(B_{3u},4)=\frac{1}{2}[U(2z)-U(3z)+U(\bar{2}z)-U(\bar{3}z)]$
	$U(B_{3u},5)=(1/8^{1/2})[U(4x)+U(4y)+U(5x)+U(5y)+U(\bar{4}x)+U(\bar{4}y)+U(\bar{5}x)+U(\bar{5}y)]$
	$U(B_{3u},6)=\frac{1}{2}[U(6x)+U(7y)+U(\bar{6}x)+U(\bar{7}y)]$
	$U(B_{3u},7)=\frac{1}{2}[U(6y)+U(7x)+U(\bar{6}y)+U(\bar{7}x)]$
	$U(B_{3u},8)=\frac{1}{2}[U(8x)+U(8y)+U(\bar{8}x)+U(\bar{8}y)]$

the other two modes the longitudinal force constants are not involved and, therefore, the transverse force constants are quite effective. Consequently, in the A_g mode one expects a localized mode, while in other modes we may get a localized mode or a resonant mode depending on the motion of the neighboring atoms of the dumbbell. If the neighbors move in phase or out of phase with the dumbbell atoms we get a resonance or localized mode accordingly. For odd-symmetry translation modes B_{1u}, B_{2u}, and B_{3u} also the nature of the characteristic mode is decided by the phase shift between motions of the dumbbell and its neighbors, i.e, these are in phase for the resonance modes and are out of phase for the localized modes.

III. APPLICATION TO Mo

We have calculated the local frequency spectrum of the dumbbell atom in Mo. In order to calculate the local spectrum we have to evaluate the force constants in the vicinity of the defect in addition to computing the ideal lattice Green's functions. For calculating force constants in the defect space we use the potential constructed by Johnson and Wilson[31] (JW) from elastic constants and unrelaxed vacancy formation energy. The JW potentials are simple and can easily be applied in defect calculations. They have been used in calculations of irradiation-produced point defects in bcc metals and give the correct trend for the properties of point defects in various bcc metals.[12] More importantly, the JW potentials clearly represent the difference in elastic property between two groups of bcc metals, i.e., between so-called normal metals α-Fe, Mo, and W and superconductors, V, Nb, and Ta, a property quite vital for the configuration and migration characteristics of SIA's in these metals. However, apart from the use of the constant unrelaxed vacancy formation energy of 1.8 eV for all the bcc metals considered, the JW potential has a shortcoming in that it leads to a very high value of activation energy of interstitial migration.[1,12] This indicates that the electronic effects might be quite important in bcc metals as many other pair potentials also fail to give low activation energies found in experiments.[1] Incidentally, the improved N-body potentials based on the embedded atom method[32] give lower values of migration energy, though still much larger than experimental values, but they fail to give the correct configuration of SIA's in Mo and W.[33] Under these circumstances, the JW potential is considered to be the only available set at present which represents the crystal properties rather well and gives the correct trend for the defect properties though some pair potentials have been constructed by a similar method. In fact, except at some high symmetry points in the first Brillouin zone, the phonon dispersion in Mo is correctly described by the JW potential.[31] Nevertheless we feel that the use of the JW potential, in general, will result in upward shift of phonon frequencies because the most dominant nearest-neighbor force constant calculated with the JW potential, $A_1^0(\mathrm{JW})=6.4578\times10^4$ dyn/cm, is much higher than that occurring in lattice dynamical model $A_1^0(\mathrm{phonons})=3.97\times10^4$ dyn/cm, fitted on the basis of the experimentally observed phonon frequencies[34] and which are to be used for the evaluation of the perfect lattice Green's functions. As far as the defect spectrum is concerned, the possible resonant-mode frequencies are likely to be overestimated because of the close correlation between the resonant modes and the migration energies of SIA's. In view of this discussion, therefore, the JW potential will be used only to estimate the relative magnitudes of different force constants in the defect space and the actual force constants to be used in the calculations will be obtained by scaling these force constants according to the lattice-dynamical force model derived on the basis of the experimental phonons.

The equilibrium position of the dumbbell is taken to be $(\pm 0.5283, \pm 0.5283, 0)a/2$ as found by Taji *et al.*[12] in molecular-dynamics simulation using the same JW potential. Having fixed the dumbbell position, we have used the Green's-function method of lattice statics to find the equilibrium positions of other atoms in the defect space.[30] The strongest distortion is suffered by four nearest neighbors of the dumbbell in the $(1\bar{1}0)$ plane, i.e., atoms 2, 3, $\bar{2}$, and $\bar{3}$ (see Fig. 1). However, in view of the known fact that the Green's-function method based on harmonic approximation underestimates the distortion nearest to the dumbbell, it was thought to be necessary to use alternative values for the displacements of these atoms. As there is no published result on the displacement field of the $\langle 110 \rangle$ dumbbell in Mo, the magnitude of distortion for

these atoms was taken to be $0.29a/2$, a value found for α-Fe in another computer simulation,[10] instead of $0.225a/2$ found for α-Fe, Mo, and W in the lattice-statics calculation.[30] In view of the fact that in the units of $a/2$, the separation between the dumbbell atoms is almost the same for all the three normal metals α-Fe, Mo, and W,[12] and the distortion of the nearest neighbors as calculated by the lattice statics is also the same ($=0.225a/2$) for all the three metals the use of α-Fe displacements is unlikely to have any important effect on the calculated force constants and on the resulting frequency spectrum. With the equilibrium position of the atoms in the defect space thus taken into account, we consider five types of force constants A_i, B_i ($i=1,\ldots,5$) corresponding to different distainces characterized by the following pairs of atoms: $(1,\bar{1})$, (1,2), (1,4), (1,6), and (1,8) (see Fig. 1). The vacancy is described by zero coupling to its neighbors. The following values of force constants are obtained:

$$\begin{aligned} &A_1=7.4714A_1^0,\quad A_2=9.1731A_1^0,\quad A_3=0.5582A_1^0\ ,\\ &A_4=2.2972A_1^0,\quad A_5=0.5309A_1^0\ ,\\ &B_1=-0.6845A_1^0,\quad B_2=-0.8838A_1^0\ ,\\ &B_3=-0.0451A_1^0,\quad B_4=-0.1634A_1^0,\quad B_5=0.0485A_1^0\ , \end{aligned} \tag{10}$$

where A_1^0 is the nearest-neighbor longitudinal force constant in the ideal lattice. The perfect lattice Green's function of Mo was calculated by a modified Gilat-Raubenheimer method[35] utilizing phonon data calculated on the basis of a third-nearest neighbor axially symmetric force model derived from Born–van-Karman fits to the measured phonons.[34] In the actual calculation of the local frequency spectrum the nearest-neighbor force constant A_1^0 for the ideal lattice figuring in Eq. (10) was set equal to that occurring in the lattice-dynamical model used for the phonon calculations. This amounts to scaling the force constants calculated on the basis of the JW potential by a factor equal to A_1^0(phonons)/A_1^0(JW) (=0.641 51). This type of procedure is essential for ensuring consistency between used phonons in the calculation of the Green's functions and the used force-constant changes in the defect space. Furthermore, this type of scaling has the effect of reducing the defect-induced phonon frequencies thus offsetting the overestimation of resonant-mode frequencies suspected with the use of the JW potential. Since the potential function corresponding to the force-constant model used for generating the perfect lattice Green's function is not known, an alternate and more consistent procedure would have been to use the same pair potential (JW) to calculate the Green's functions. However, is using phonon-based force constants for the Green's functions, the idea is to ensure that the perfect crystal is correctly described within the harmonic approximation and possible uncertainties remain confined to the force constants in the vicinity of the defect alone. In any case, after the scaling of the force constants according to the lattice-dynamical model, clearly a consistency has been achieved between the force constants used for Green's functions and the force constants in the vicinity of the defect.

The calculated local frequency spectrum of the dumbbell atom and the host lattice spectrum are plotted in Fig. 3. The characteristic feature of the defect spectrum is the occurrence of sharp resonance modes within the allowed band of frequencies and localized vibrational modes above the crystal maximum frequency $\omega_{\max}$. As a matter of fact, the defect spectrum is described by resonant and localized modes alone with little participation of the normal modes of the host lattice. There are in all six resonance modes, five at low frequencies and a resonance mode of B_{1g} symmetry just below the band edge. The frequencies of the resonance modes are (in THz)

$$\begin{aligned} &\nu_r^{B_{1g}}=1.39,\quad \nu_r^{B_{3u}}=2.59,\quad \nu_r^{B_{2g}}=2.73\ ,\\ &\nu_r^{B_{2u}}=2.83,\quad \nu_r^{B_{1u}}=3.29,\quad \nu_r^{B_{1g}}=7.995\ . \end{aligned} \tag{11}$$

There are six localized modes one of which is just above $\omega_{\max}$. The frequencies are

$$\begin{aligned} &\nu_l^{A_g}=8.26,\quad \nu_l^{B_{2u}}=8.07,\quad \nu_l^{B_{3u}}=10.965\ ,\\ &\nu_l^{B_{2g}}=12.17,\quad \nu_l^{B_{1u}}=12.38,\quad \nu_l^{A_g}=12.77\ . \end{aligned} \tag{12}$$

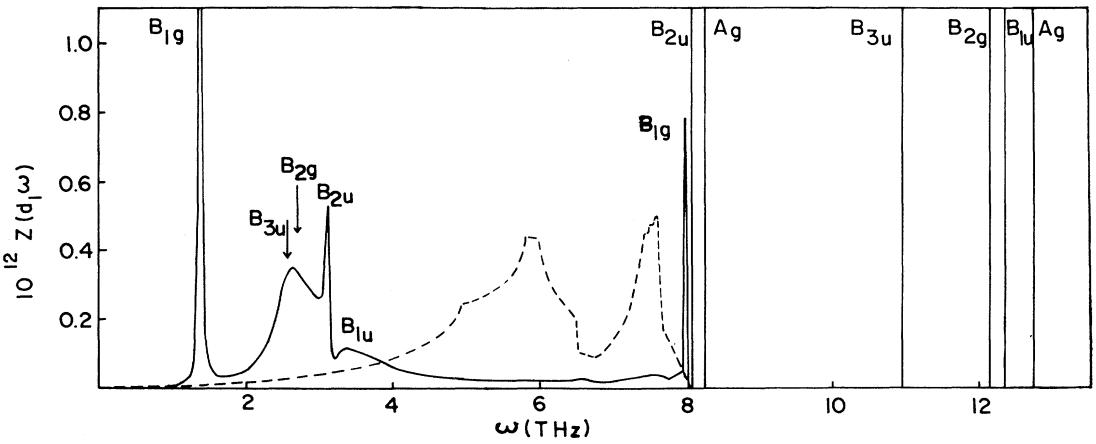

FIG. 3. Local frequency spectra of the ⟨110⟩ dumbbell (——) and an atom in the host lattice (— — —).

The spectrum shows that the vibration amplitudes of the dumbbell are much larger than the host atoms with dominant contributions from x and y components. Especially large amplitudes are observed for sharp resonance modes B_{1g} and B_{2u} having displacements along $[1\bar{1}0]$. Comparitively smaller amplitudes are seen for broader resonance modes B_{2g} and B_{1u} with dumbbell displacement along [001]. For the breathing mode A_g and the translation mode B_{3u} the interstitial atoms move along dumbbell axis [110]. The amplitude distribution in different modes can be understood from the following considerations. For motion along $[1\bar{1}0]$ the dominant longitudinal force constants are not involved at all and the effect of negative transverse force constants B_1 and B_2 is maximum whereas for motion along [001] the transverse force constant B_2 is less effective and in addition the longitudinal force constant A_2 between the dumbbell atom and its neighbors in the $(1\bar{1}0)$ plane is also involved (see Fig. 2). We observe that for the breathing mode A_g the longitudinal force dumbbell atoms is effective and the relatively weak transverse force is not important leading to a localized mode, whereas in the case of resonance modes—both for the translation modes with odd symmetry as well as the libration modes with even symmetry—the neighboring atoms move in phase with dumbbell atoms so that connecting strong longitudinal forces are not effective and consequently the mode frequency is lowered.

The resonance modes lead to large mean-squre thermal displacements of the interstitial

$$\langle u_\alpha^2 \rangle = \int \frac{Z_\alpha(d,\omega)}{2M\omega} \coth\left[\frac{\hbar\omega}{2kT}\right] d\omega \ , \tag{13}$$

which become proportional to T at high temperatures

$$\langle u_\alpha^2 \rangle = kTG_{\alpha\alpha}(d,d;\omega=0), \ kT > h\omega_r \ . \tag{14}$$

The calculated mean-squre thermal displacement for a dumbbell atom and for a host atom are given in Fig. 4. For $T>40$ K, $\langle u^2 \rangle$ for the dumbbell atom increases more rapidly than that for the host atom and varies linearly with T. This is consistent with a Mössbauer study of trapped interstitials at ^{57}Co by Marangos *et al.*[25] These authors concluded that the defect complex is the $\langle 110 \rangle$ dumbbell with one of the neighbors being substitutional ^{57}Co and have found that there is a strong increase of mean-square thermal displacement of Mössbauer impurity at about $0.1\Theta_D (=40.3$ K) and, therefore, for a detailed comparison with the experiment the appropriate quantity is the thermal displacement squared of one of the neighbors of the dumbbell. However, a comparison is still possible, since in a resonance mode the motion of the neighbors is in phase with that of the dumbbell atom and thus the same resonance is involved in the vibrations of the dumbbell as well as the neighboring ^{57}Co atom. To the extent that the thermal population of resonance modes is responsible for the strong increase of $\langle u^2 \rangle$ at 40 K and its linear increase with T above this temperature, the present result of mean-square thermal displacement is essentially in agreement with the experiment as a strong increase of $\langle u^2 \rangle$ of the substitutional ^{57}Co atom as well as that of the dumbbell atom at about the same temperature of 40 K is indicative of the interstitial diffusion stage I_D. In fact, the temprature 40 K nearly coincides with the interstitial diffusion state I_D in Mo.[36]

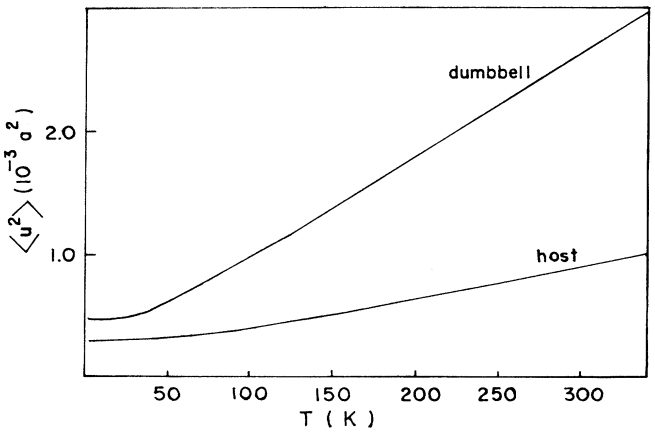

FIG. 4. Mean-square thermal displacements for a $\langle 110 \rangle$-dumbbell atom and for an atom in the host lattice.

Because of resonance modes the SIA's show large dia-elastic polarizability. The influence of resonance modes on elastic constants is determined, to a large extent, by selection rules based on symmetry. The most important contribution to the change of elastic moduli is given by[2]

$$\Delta C^\rho = \frac{c}{V_c} \langle \epsilon^\rho R \, | t(0) | \epsilon^\rho R \rangle \ , \tag{15}$$

where ϵ^ρ are eigenstrains, R is the position vectors of atoms, $t(0)$ is the t matrix in the static limit, V_c is the unit cell volume, and c is the concentration of defects. Using symmetry coordinates and appropriate eigenstrains we find that changes in different elastic moduli $\Delta(C_{11}+2C_{12})$, $\Delta(C_{11}-C_{12})$, and $\Delta(2C_{44})$ are determined by t^{A_g}, $(t^{A_g}, t^{B_{1g}})$, and $(t^{A_g}, t^{B_{2g}}, t^{B_{3g}})$, respectively. Since the A_g mode gives only localized modes the bulk effect is seen to be small and, therefore, in the presence of sharp dumbbell resonances, it is clear that $\Delta(C_{11}-C_{12})$ and $\Delta(2C_{44})$ are determined by librational modes B_{1g} and B_{2g}, respectively. For resonance modes the t matrix is approximated by[2]

$$t(0) = V - V\frac{|r\rangle\langle r|}{M\omega_r^2}V = -V\frac{|r\rangle\langle r|}{M\omega_r^2}V \ , \tag{16}$$

where $V=\Phi-\Phi^0$ is the force-constant change matrix pertaining to the entire defect space and $|r\rangle$ represents the normalized resonance state. From Eqs. (15) and (16) it is evident that, in the event of resonant contribution to the elastic constants, the change is always negative. Especially, the reduction in the shear moduli is inversely proportional to the square of the resonant frequency and it becomes very large for low-frequency dumbbell resonance. As $\omega_r^{B_{1g}} < \omega_r^{B_{2g}}$ we conclude that $-\Delta C' > -\Delta C_{44}$. This is in agreement with the experimental measurements of Okuda and Mizubayashi.[27]

The long-range migration of SIA's can be explained in terms of the resonant modes. By sufficient thermal excitation of the resonant modes the dumbbell atoms acquire enough energy to overcome the saddle point forming a new dumbbell with one of the neighboring atoms. An inspection of Fig. 2 shows that purely translational mode B_{3u} may give rise to one-dimensional migration whereas the librational modes B_{1g} and B_{2g} may cause rotations by 90° in the (001) plane and by 60° in the (111) plane, respectively. The long-range migration is possible through a combination of the translation and one of the rotations. However, migration in the (001) plane, either through pure translation or through a combination of the translation (B_{3u}) and the rotation by 90° (B_{1g}), is unlikely since such jumps involve distances larger than the nearest-neighbor distance in the lattice. Threfore the long-range migration of SIA's should occur through the combination of the translation B_{3u} and the libration B_{2g}. However, there could be two possible mechanisms: (i) a three-dimensional migration with a reorientation of the dumbbell axis by 60°, a process found in computer simulation[1,12] and (ii) a two-dimensional migration without reorientation in which the dumbbell jumps to a neighboring site while its axis remains in the $(1\bar{1}0)$ plane. Similar to the elementary jump of the ⟨100⟩ dumbbell in fcc metals one would suspect that the jumping process involving the reorientation of the ⟨110⟩ dumbbell should be favorable. However, in elastic aftereffect measurements a reorientation of the ⟨110⟩ dumbbell has not been observed up to 500 K.[26] We conclude, therefore, that a two-dimensional jump through the combined effect of the B_{3u} translation and the B_{2g} libration provides a consistent picture of the long-range migration of SIA's in Mo. Thus unlike the ⟨100⟩ dumbbell in fcc metals, where the libration E_g is involved in both the long-range migration of SIA's as well as strongest softening of the lattice, in the present case two different libration modes of the ⟨110⟩ dumbbell are involved in these phenomena, i.e., while B_{2g} is involved in the long-range migration of SIA's the B_{1g} mode has the lowest frequency and causes the strongest softening of the lattice.

We note that one shortcoming in the calculation is the use of the JW potential. Nevertheless, the calculated local frequency spectrum gives an excellent account of experimental results in Mo and we feel that the broad features of the spectrum are unlikely to be changed with an improved potential.

IV. CONCLUSION

We have discussed the dynamics of self-interstitial atoms in bcc metals with the use of the Green's-function method. Employing a second-nearest-neighbor defect model, we have discussed the conditions for the occurrence of the resonant and localized modes of ⟨110⟩-split-interstitial atoms. We have shown that the local frequency spectrum of the ⟨110⟩-split-interstitial atoms in bcc metals is described by resonant and localized modes alone and an almost negligible contribution comes from the eigenfrequencies of the perfect lattice. In agreement with experiment the spectrum leads to much enhanced thermal displacements of the defect. The calculated resonance frequencies of librational modes B_{1g} and B_{2g} provide consistent explanation of observed changes of shear moduli in irradiated Mo. The long-range migration of SIA's in bcc metals results from two-dimensional jumps of ⟨110⟩ dumbbells in their (110) habit planes which is made possible though the combined effect of the translational mode B_{3u} and the librational mode B_{2g}. The result for the vibrations of the ⟨110⟩ dumbbell in bcc metals is very similar to that of the ⟨100⟩ dumbbell in fcc metals. However, there is an important difference: while in fcc metals the librational mode E_g of the ⟨100⟩ dumbbell figures in both the long-range migration of SIA's as well as the strongest softening of the lattice, in bcc metals two different librational modes of the ⟨110⟩ dumbbell figure in these processes, i.e., the long-range migration of SIA's is helped by the B_{2g} mode but the strongest softening of the lattice is caused by the librational mode B_{1g}. Finally, the present result for the ⟨110⟩-dumbbell vibrations are considered to be typical of bcc metals.

ACKNOWLEDGMENTS

The author is grateful to University Grants Commission, New Delhi for financial assitance and to Dr. H. R. Schober for sending the Green's-function program.

[1]P. H. Dederichs, C. Lehmann, H. R. Schober, A. Scholz, and R. Zeller, J. Nucl. Mater. **69&70**, 176 (1978).
[2]P. H. Dederichs and R. Zeller, in *Point Defects in Metals II,* edited by G. Höhler and E. A. Niekisch, Springer Tracts in Modern Physics Vol. 87 (Springer, Berlin, 1980).
[3]W. Schilling, J. Nucl. Mater. **69&70**, 465 (1978).
[4]F. W. Young, Jr., J. Nucl. Mater. **69&70**, 310 (1978).
[5]P. H. Dederichs, C. Lehmann, and A. Scholz, Phys. Rev. Lett. **31**, 1130 (1973).
[6]H. R. Schober, V. K. Tewary, and P. H. Dederichs, Z. Phys. B **21**, 255 (1975); R. F. Wood and M. Mostoller, Phys. Rev. Lett. **35**, 45 (1975); R. Zeller and P. H. Dederichs, Z. Phys. B **25**, 139 (1976).
[7]P. N. Ram and P. H. Dederichs, Z. Phys. B **42**, 57 (1981); Kernforschungsanlage Jülich Report No. Jül. 1725, 1981 (unpublished).
[8]P. N. Ram, Phys. Rev. B **30**, 6146 (1984); **37**, 6783 (1988); J. Phys. F **15**, 35 (1985).
[9]R. Urban, P. Ehrhart, W. Schilling, H. R. Schober, and H. Lauter, Mater. Sci. Forum. **15 - 18**, 243 (1987); Phys. Status Solidi B **144**, 287 (1987).
[10]C. Erginsoy, G. H. Vineyard, and A. Englert, Phys. Rev. **133**, A595 (1964).
[11]R. A. Johnson, Phys. Rev. **134**, A1329 (1964).
[12]Y. Taji, T. Iwata, T. Yokota, and M. Fuse, Phys. Rev. B **39**, 6381 (1989).
[13]K. M. Miller, J. Phys. F **11**, 1175 (1981).
[14]M. W. Guinan, R. N. Stuart, and T. J. Borg, Phys. Rev. B **15**,

699 (1977).
[15]P. Ehrhart, J. Nucl. Mater. **69&70**, 200 (1978).
[16]P. Ehrhart, Brit. Nucl. Energy Soc. **1**, 101 (1983).
[17]G. Wallner, H. Franz, R. Rauch, A. Schmalzbauer, and J. Peisel, Mater. Sci. Forum **15-18**, 907 (1987).
[18]S. Okuda and H. Mizubayashi, Cryst. Lattice Defects **4**, 75 (1973); Radiat Eff. **33**, 221 (1977).
[19]J. A. Dicarlo, C. L. Snead, Jr., and A. N. Goland, Phys. Rev. **178**, 1059 (1969); S. Okuda and H. Mizubayashi, Phys. Rev. B **13**, 4207 (1976); J. R. Townsend, M. Schilderout, and C. Reft, *ibid.* **14**, 500 (1976).
[20]V. Hivert, R. Pichon, H. Bilger, P. Bichon, J. Verdone, D. Dautreppe, and P. Moser, J. Phys. Chem. Solids **31**, 1843 (1970).
[21]W. Chambrone, J. Verdone, and P. Moser, in *Proceedings of the Conference on Fundamental Aspects of Radiation Damage in Metals, Gatlinburg, 1975,* edited by M. T. Robinson and F. W. Young, Jr. (U.S. Department of Commerce, Springfield, Virginia, 1976), p. 261.
[22]H. Mizubayashi and S. Okuda, Radiat. Eff. **54**, 201 (1981).
[23]H. E. Schaefer, D. Butteweg, and W. Dander, in Ref. 21, p. 463; M. Hirscher, B. Schwendemann, and H. Kronmuller, Cryst. Lattice Defects Amorph. Mater. **11**, 245 (1985).
[24]P. Lucasson, F. Maury, and A. Lucasson, Mater. Sci. Forum **15-18**, 231 (1987).
[25]J. Marangos, W. Mansel, and D. Wahl, Mater. Sci. Forum **15-18**, 225 (1987).
[26]H. Jacques and K. H. Robrock, in *Point Defects and Defect Interactions in Metals,* edited by J. Takamura, M. Doyama, and M. Kiritani (University of Tokyo Press, Tokyo, 1982), p. 159.
[27]S. Okuda and H. Mizubayashi, in Ref. 26, p. 163.
[28]H. Schultz, Mater. Sci. Forum. **15-18**, 727 (1987).
[29]W. Frank and A. Seeger, Mater. Sci. Forum **15-18**, 57 (1987).
[30]P. N. Ram, Phys. Rev. B, **43**, 6480 (1991).
[31]R. A. Johnson and W. D. Wilson, in *Interatomic Potentials and Simulation of Lattice Defects,* edited by P. C. Gehlen, J. R. Beeler, Jr., and R. I. Jaffee (Plenum, New York, 1972), p. 301.
[32]M. S. Daw and M. I. Baskes, Phys. Rev. B **29**, 6443 (1984); M. W. Finnis and J. E. Sinclair, Philos. Mag. A **50**, 45 (1984).
[33]A. H. Foster, J. M. Harder, and D. J. Bacon, Mater. Sci. Forum **15-18**, 849 (1987); G. J. Ackland and R. Thetford, Philos Mag. A **56**, 15 (1987); J. M. Harder and D. J. Bacon, *ibid.* **58**, 165 (1988).
[34]A. D. B. Woods and S. H. Chen, Solid State Commun. **2**, 233 (1964).
[35]G. Gilat and L. J. Raubenheimer, Phys. Rev. **144**, 390 (1966).
[36]H. Kugler, J. A. Schwirtlich, S. Takaki, V. Ziebart, and H. Schultz, in Ref. 26, p. 191.